CrystEngComm

Dynamic Characterization of Crystalline Fluorophores with Conformationally Flexible Tetrahydrocarbazole Frameworks

Journal:	*CrystEngComm*
Manuscript ID	CE-ART-03-2020-000423.R1
Article Type:	Paper
Date Submitted by the Author:	23-Apr-2020
Complete List of Authors:	Colin-Molina, Abraham; Instituto de Quimica UNAM, Quimica Organica Velazquez-Chavez, Diego; Instituto de Quimica UNAM, Quimica Organica Jellen, Marcus; University of California Los Angeles, Chemistry and Biochemistry Rodríguez-Cortés, Lizbeth; Instituto de Quimica UNAM, Quimica Organica Cifuentes Quintal, Miguel Eduardo; Cinvestav-Mérida, Department of Applied Physics Merino, Gabriel; Centro de Investigación y de Estudios Avanzados, Applied Physics Rodríguez-Molina, Braulio; Instituto de Quimica UNAM, Quimica Organica

ARTICLE

Dynamic Characterization of Crystalline Fluorophores with Conformationally Flexible Tetrahydrocarbazole Frameworks

Received 00th January 20xx,
Accepted 00th January 20xx

DOI: 10.1039/x0xx00000x

Abraham Colin-Molina,[a] Diego Velázquez-Chávez,[a] Marcus J. Jellen,[b] Lizbeth A. Rodríguez-Cortés,[a] Miguel Eduardo Cifuentes-Quintal,[c] Gabriel Merino,[c] and Braulio Rodríguez-Molina.[a,*]

Two new compounds **2** and **3** and their deuterated analogues **2-*d*$_4$** and **3-*d*$_4$** have been prepared from Ullmann-type coupling reactions. Both showed good emissive properties in solution Φ_F = 0.13 (**2**) and 0.57 (**3**) as well as in the solid-state (Φ_F = 0.35 and 0.33, respectively). Variable temperature solid-state NMR measurements using ^{13}C CPMAS and ^{2}H spin-echo helped to identify segmental motion in the phenylene as well as in the aliphatic moieties, which agrees well with the crystallographic disorder in these moieties. The rotational energy barriers E_a for the new compounds were obtained with periodic DFT computations, finding asymmetric rotational potentials with barriers of 3.5 kcal/mol (**2**) and 4.5 kcal/mol (**3**) for 60° jumps and much higher barriers (> 25 kcal/mol) for 180º jumps. Our studies indicate that low frequency 4-fold motions coexist with fluorescence in these crystalline conjugated compounds.

Introduction

Crystalline molecular rotors are artificial molecular machines designed to display intramolecular rotation that resembles the motion of macroscopic gears and spurs.[1-3] These compounds can be synthesized by connecting at least three molecular components: a bulk moiety with a large moment of inertia that dictates the crystalline array (framework), a mobile component that reorients under an appropriate stimulus (rotator), and the linker between the two (axle).[4] Using principles borrowed from crystal engineering, numerous reports have laid down many synthetic strategies from discrete molecules to embed rotors in porous frameworks with free space to facilitate motion within crystals.[5-11]

One of the many exciting challenges in this field is to design crystalline materials akin to molecular rotors, that feature good solid-state emission and thus can be employed in optoelectronic devices.[12-15] The combination of these properties is attractive because very fast molecular motions can act as the non-radiative channel to relax the excited states of conjugated molecules, allowing them to exert control of the fluorescent properties of crystals by turning on and off their intramolecular dynamics.

A strong correlation between motion and emission has already been hypothesized to describe the behaviour of conjugated twisted compounds that are not emissive in solution but highly emissive in the solid-state. This phenomenon, termed Aggregation-Induced Emission (AIE),[16-18] invokes the restriction of intramolecular rotations (RIR) or vibrations (RIV) as the underlying mechanisms for such behaviour, although very few studies are focused on the dynamic characterization have been reported.[19]

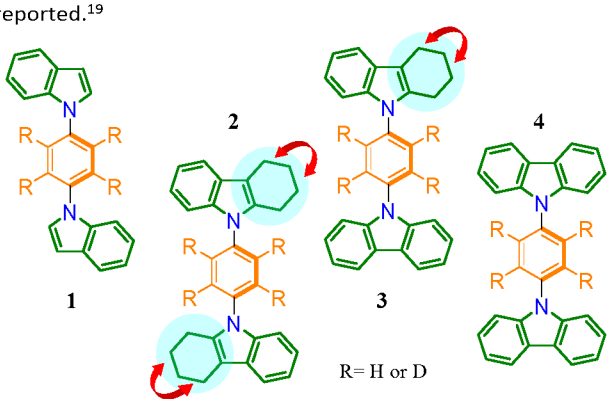

Figure 1. Molecular structures of the compounds **1**, **2**, **3**, and **4** compared in this manuscript.

With this in mind, determining the internal motion (or the absence of it) in crystalline molecules with solid-state fluorescence is a great opportunity to learn more about these properties. As a starting point, attention was paid to compound **1** (indole-phenylene-indole framework), which was reported as

[a] *Instituto de Química, Universidad Nacional Autónoma de México, Circuito Exterior, Ciudad Universitaria, Ciudad de México, 04510, México.*
[b] *Department of Chemistry and Biochemistry, University of California, Los Angeles, California 90095, United States.*
[c] *Departamento de Física Aplicada, Centro de Investigación y de Estudios Avanzados, Unidad Mérida. Km 6 Antigua Carretera a Progreso. Apdo. Postal 73, Cordemex, 97310, Mérida, Yuc., México.*

Electronic supplementary information (ESI) available: Fig. S1–S26 and crystal structures of 2 and 3 in CIF format. CCDC numbers are 1990760 (**2**)/1990761 for (**3**) at 298 K and 1998402 (2) at 100 K.

an AIE compound, although no dynamic characterization was provided.[20] The structural similarity of **1** with compound **4** (carbazole-phenylene-carbazole), which has very low solid-state emission and no intramolecular rotation,[21] motivated the development of the new compounds described here as an attempt to find how to balance these properties.

In this work, we changed the rigid carbazole moiety for tetrahydrocarbazole (TCz), a flexible framework where one of the fused rings is now aliphatic. Such modification is included to increase the degrees of freedom in the solid-state in these molecules, changing the resulting motion and emissive properties. Therefore, we report here the synthesis, characterization, and solid-state dynamics of compound **2** with two TCz components, and compound **3** with one TCz and one carbazole framework surrounding a central phenylene (Figure 1).

Compounds **2** and **3** produce isomorphous fluorescent crystals, with comparable good quantum yields **2** (ϕ = 0.35) and **3** (ϕ = 0.33). Variable temperature solid-state NMR ^{13}C CPMAS corroborates the flexibility of the TCz components. Interestingly, these degrees of freedom of the framework allow the motion of the central phenylene at room temperature, as confirmed by variable-temperature solid-state ^{2}H NMR experiments using isotopically enriched analogues. Density functional theory (DFT) computations further studied the complex internal motion. Our findings indicate that solid-state emission and internal motion can coexist in the solid-state in these heterocyclic structures.

Experimental

Materials and methods

All reagents were purchased from Sigma-Aldrich and used as received. THF was dried before use by distillation over Na/benzophenone. Flash column chromatography was performed using silica gel Aldrich 230-400 mesh. Reactions were monitored by TLC on silica gel plates 60 F_{254} (Merck) and spots were detected by UV-absorption. ^{1}H and ^{13}C NMR spectra of all compounds were recorded at ambient temperature using Bruker Fourier300 and Jeol Eclipse 300, and they are referenced to $CDCl_3$ (7.26 ppm, 77.0 ppm), as indicated. The FT-IR spectral data were recorded with Bruker ATR in the 450-4000 cm^{-1} range. Melting points were determined by Differential Scanning Calorimetry. HRMS were obtained by Direct Analysis in Real Time (DART) in AccuTOF, JMS-T100LC. A detailed description of the general methods can be seen in the ESI.

Synthesis and characterization

Compound 1-*d*$_4$. 0.400 g (1 eq, 1.20 mmol) of 1,4-diiodobenzene-d_4, 0.420 g (3 eq, 4.80 mmol) of indole, 0.023 g (0.1 eq, 0.12 mmol) of CuI, 0.016 g (0.05 eq, 0.06 mmol) of 18-crown-6 and 0.410 g (2.5 eq, 3 mmol) of K_2CO_3 were placed in a two-neck round bottom flask with 3 mL of DMPU. The reaction mixture was deoxygenated with N_2 and heated to 140 °C for 12 h. The crude of the reaction was poured into saturated NH_4Cl solution and the solid was filtered, dried, and purified by column chromatography using hexane/DCM (95:5) as eluent to give the product as a white solid (0.190 g, yield 52%, m.p. 295.4 °C determined by DSC). ^{1}H NMR (300 MHz, $CDCl_3$) δ: 7.77 (d, *J*=8 Hz, 2H), 7.68 (d, *J*=8 Hz, 2H), 7.43 (d, *J*=3 Hz, 2H), 7.23-7.75 (m, 4H), 6.78 (d, *J*=3 Hz, 2H). ^{13}C NMR (75 MHz, $CDCl_3$) δ: 137.8, 135.9, 129.4, 127.9, 125.0, 122.7, 121.3, 120.6, 110.4, 104.1. FT-IR (ATR, cm^{-1}) *v*= 3055.4, 1515.4, 1466.1, 1203.5, 741.8, 714.1. HRMS (DART) $C_{22}H_{13}D_4N_2$ m/z calc= 313.16373, found=313.16263 diff. (ppm)= 3.51.

Compound 2. 0.400 g (1 eq, 1.21 mmol) of 1,4-diiodobenzene, 0.620 g (3 eq, 3.63 mmol) of 1,2,3,4-tetrahydrocarbazole, 0.023 g (0.1 eq, 0.12 mmol) of CuI, 0.013 g (0.05 eq, 0.06 mmol) of 18-crown-6 and 0.500 g (3 eq, 3.63 mmol) of K_2CO_3 were placed in a two-neck round bottom flask with 3 mL of DMPU. The reaction mixture was deoxygenated with a flux of N_2 and heated to 160 °C for 24 h. After the reaction time, the crude of the reaction was cooled to room temperature and poured into a saturated solution of NH_4Cl. The solid obtained was filtered, dried and purified by column chromatography using Hexane/DCM (97:3) to obtain the product as a white solid (0.300 g, yield 60%, m.p. 300.8 °C determined by DSC). ^{1}H NMR (400 MHz, $CDCl_3$) δ: 7.58-7.56 (m, 2H), 7.52 (s, 4H), 7.37-7.35 (m, 2H), 7.19-7.17 (m, 4H), 2.85 (s, 4H), 2.72 (s,4H), 1.96 (s, 8H). ^{13}C NMR (100 MHz, $CDCl_3$) δ: 137.1, 136.6, 135.7, 127.9, 127.8, 121.5, 119.8, 117.9, 111.4, 109.8, 23.4, 23.1, 21.1. FT-IR (ATR, cm^{-1}) *v*= 3043.2, 2918.8, 2832.5, 1513.8, 1456.5, 1370.7, 1230.4, 826.8, 740.5. HRMS (DART) $C_{30}H_{29}N_2$ m/z calc= 417.23307, found=417.23336 diff. (ppm)= 0.70.

Compound 2-*d*$_4$. The same procedure for **2** was followed with the next quantities: 0.300 g (1 eq, 0.89 mmol) of 1,4-diiodobenzene-d_4, 0.460 g (3 eq, 2.69 mmol) of 1,2,3,4-tetrahydrocarbazole, 0.017 g (0.1 eq, 0.09 mmol) of CuI, 0.012 g (0.05 eq, 0.04 mmol) of 18-crown-6 and 0.370 g (3 eq, 3.63 mmol) of K_2CO_3. White solid (0.21 g, yield 56%). ^{1}H NMR (400 MHz, $CDCl_3$) δ: 7.67-7.65 (m, 2H), 7.46-7.43 (m, 2H), 7.27-7.25 (m, 4H), 2.93 (s, 4H), 2.79 (s,4H), 2.04 (s, 8H). ^{13}C NMR (100 MHz, $CDCl_3$) δ: 137.2, 136.5, 135.8, 128.0, 127.5, 121.6, 119.9, 118.0, 111.5, 109.9, 23.5, 23.2, 21.2. FT-IR (ATR, cm^{-1}) *v*= 3042.2, 2919.7, 2834.4, 1461.3, 1301.3, 1228.5, 739.1, 726.1, 447.9. HRMS (DART) $C_{30}H_{25}D_4N_2$ m/z calc= 421.25818, found=421.25786 diff. (ppm)= 0.77.

Compound 3. 0.400 g (1 eq, 1.08 mmol) of *N*-(4-Iodophenyl)carbazole, 0.370 g (2 eq, 2.16 mmol) of 1,2,3,4-tetrahydrocarbazole, 0.020 g (0.1 eq, 0.10 mmol) of CuI, 0.014 g (0.05 eq, 0.05 mmol) of 18-crown-6 and 0.220 g (1.5 eq, 1.62 mmol) of K_2CO_3 were placed in a two-neck round bottom flask with 3 mL of DMPU. The reaction mixture was deoxygenated with N_2 and heated to 160 °C for 15 h. The crude of the reaction was poured into saturated NH_4Cl solution and the crashing solid was filtered, dried and purified by column chromatography using Hexane/DCM (95:5) as eluent to give the product as a white solid (0.280 g, yield 64%, m.p. 295.4 °C determined by DSC). ^{1}H NMR (400 MHz, $CDCl_3$) δ: 8.22 (d, *J*=8 Hz, 2H), 7.75 (d, *J*=8 Hz, 2H), 7.64 (d, *J*=8 Hz, 3H), 7.57 (d, *J*=8 Hz, 2H), 7.50 (t, 2H), 7.46-7.44 (m, 1H), 7.37 (t, 2H), 7.23-7.22 (m, 2H), 2.86 (s, 2H), 2.76 (s, 2H), 1.98 (s, 4H). ^{13}C NMR (100 MHz, $CDCl_3$) δ: 140.8, 137.2, 137.0, 136.3, 135.8, 128.4, 128.0, 127.8, 126.1, 123.5,

121.6, 120.4, 120.2, 119.9, 118.0, 111.6, 109.8, 109.8, 23.5, 23.1, 21.2. FT-IR (ATR, cm^{-1}) ν= 3044.1, 2921.2, 2833.0, 1514.4, 1450.2, 1333.6, 1229.4, 743.4, 723.2. HRMS (DART) $C_{30}H_{25}N_2$ m/z calc= 413.20177, found=413.20220 diff. (ppm)= 1.02.

Compound 3-d_4. The same procedure was followed using the next amounts: 0.400 g (1 eq, 1.07 mmol) of *N*-(4-Iodophenyl)carbazole-d_4, 0.360 g (2 eq, 2.14 mmol) of 1,2,3,4-tetrahydrocarbazole, 0.020 g (0.1 eq, 0.10 mmol) of CuI, 0.014 g (0.05 eq, 0.05 mmol) of 18-crown-6 and 0.220 g (1.5 eq, 1.60 mmol) of K_2CO_3. A white solid was obtained (0.250 g, yield 58%). ^{1}H NMR (400 MHz, $CDCl_3$) δ: 8.22 (d, *J*=8 Hz, 2H), 7.62-7.61 (m, 1H), 7.57 (d, *J*=8 Hz, 2H), 7.50 (t, 2H), 7.46-7.44 (m, 1H), 7.37 (t, 2H), 7.23-7.22 (m, 2H), 2.90 (s, 2H), 2.79 (s,2H), 2.01 (s, 4H). ^{13}C NMR (100 MHz, $CDCl_3$) δ: 140.7, 137.1, 136.8, 136.1, 135.7, 1282, 127.9, 127.7, 126.0, 123.5, 121.6, 120.4, 120.2, 119.9, 117.9, 111.5, 109.8, 109.7, 23.4, 23.1, 21.1. FT-IR (ATR, cm^{-1}) ν= 3045.2, 2925.2, 2836.6, 1459.3, 1228.9, 745.2, 722.8, 450.0. HRMS (DART) $C_{30}H_{21}D_4N_2$ m/z calc= 417.22688, found=417.22688 diff. (ppm)= 0.82.

Results and Discussion

Synthesis and X-ray crystallographic studies of 2 and 3

The synthetic routes to compounds **2** and **3**, and their deuterated analogues **2-d_4** and **3-d_4**, are shown in Scheme 1. Both were prepared through an Ullmann coupling reaction using 1,4-diiodobenzene (or 1,4-diiodobenzene-d_4) or *N*-(4-iodophenyl)carbazole (**5**)[21] and 1,2,3,4-tetrahydrocarbazole (TCz) in DMPU as the solvent (experimental details and characterization are presented in the experimental section of this manuscript). Compounds **1, 4**, and **4-d_4** were synthesized following the methodology reported in the literature and characterization data was verified.[20,21]

Scheme 1. Synthetic procedure to obtain title compounds **2** and **3**

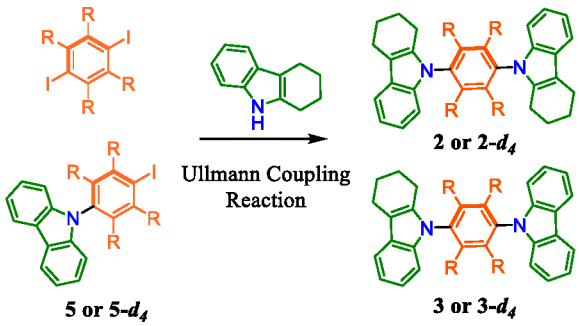

Single crystals of **2** and **3** suitable for X-ray diffraction were obtained from the slow evaporation of saturated solutions in tetrahydrofuran as prismatic crystals and the crystallographic parameters at room temperature are showed in Table 1.

Table 1. Crystallographic parameters of **2** and **3** recorded at 298 K

Compound	2	3
Formula	$C_{30}H_{28}N_2$	$C_{30}H_{24}N_2$
Molecular weight	416.54	412.51
Crystal system	monoclinic	monoclinic
Space group	$P\,2_1/n$	$P\,2_1/n$
a (Å)	11.6447(11)	11.5168(10)
b (Å)	7.7550(7)	7.6482(6)
c (Å)	12.7909(13)	12.8491(11)
α (deg)	90	90
β (deg)	90.806(3)	90.876(3)
γ (deg)	90	90
V (Å^3)	1154.96(19)	1131.65(16)
Z	2	2
Color	colorless	colorless
Crystal size (mm^3)	0.382x0.369x0.290	0.386x0.344x0.127
ρ_{calc} (g/cm^3)	1.198	1.211
μ/mm^{-1}	0.070	0.071
F (000)	444.0	436.0
Radiation (Å)	Mo $k\alpha$=0.71073	Mo $k\alpha$=0.71073
Reflns collected	14258	19288
Final R indexes [$I\geq2(I)$]	R= 0.0956 wR2= 0.2974	R= 0.0676 wR2= 0.1967

The structural differences of the framework in **2** and **3** do not play a significant role in the crystallization, in fact, both structures adopt a similar conformation (Figure S1), crystallizing in a monoclinic $P2_1/n$ space group with identical cell parameters. In the case of **2**, a dihedral angle of 54.1° is found between the central phenylene and the tetrahydrocarbazole framework, while for compound **3,** this angle is 51.9°. The asymmetric unit in both compounds is half a molecule ($Z' = 0.5$), with an inversion point residing in the phenylene centroid.

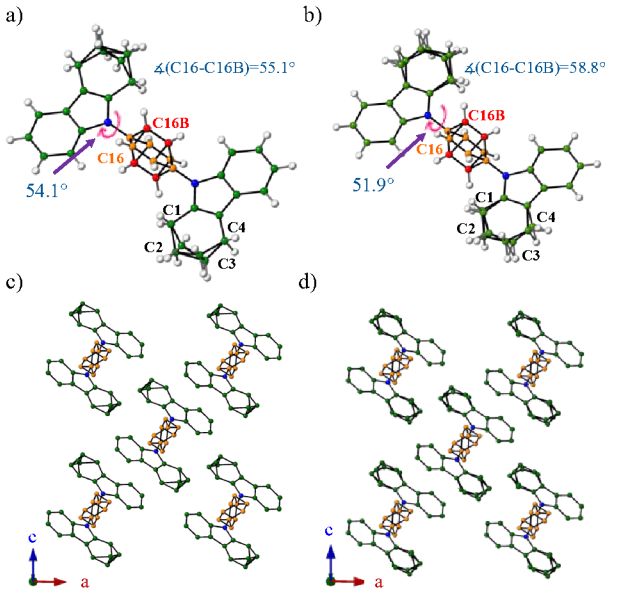

Figure 2. The dihedral angle between central phenylene and TCz frameworks and disorder positions, crystal structure viewed along the *b* crystallographic axis with ellipsoids at 30 % of probability for compound **2** (a, c) and compound **3** (b, d).

The central ring in **2** shows two disordered positions with occupancies 0.550(8) and 0.450(8) separated by angular displacement of 55.1°. Similar disordered positions are found in the structure of **3** with an angular displacement of 58.8° and occupancies of 0.612(5) and 0.388(5). The aliphatic moiety in the frameworks (labeled C1, C2, C3, and C4) is also disordered, suggesting a rapid reorganization of those atoms at room temperature (Figure 2a,b). To explore whether the disorder is dynamic and could be reduced at low temperature, the crystal structure of **2** was also determined at 100 K, but given the fact that the phenylene ring lies on a special crystallographic position, the disorder remained in two positions with similar occupancies 0.537(3) and 0.463(3) (Figure S2). Considering the structural similarity, the same result was expected for compound **3** and, thus, it was not collected at that temperature.

The crystalline packing in compounds **2** and **3** are practically the same, with comparable packing coefficients (0.677 and 0.667, respectively). These values suggest that the packing is slightly more compact in the latter, likely due to the flat nature of the aromatic framework (Figure 2c,d). The most notorious interactions in **1-4** are C-H···π contacts between central phenylene and the aromatic ring of the 1,2,3,4-tetrahydrocarbazole frameworks (Figure S3). Typically, this distance is less than 2.9 Å and has an energy value between 1.5-3 kcal mol^{-1}.[22] The distances for this interaction are 2.729 Å (for **2**) and 2.668 Å (for **3**), as indicated in Figures 3a and 3b. These interactions propagate along *b*-axis with the molecules arranged in a columnar disposition (with weak π-π stackings in **1** and **4**), given that the intermolecular centroid-centroid distance exceeds the accepted value (3.8 Å)[23] in **2** and **3** (Figure S4). A Hirschfeld surface analysis carried out for both compounds revealed similar critical points and fingerprints, indicating that the C-H···π interactions (with de+di≈2.6 Å, which is close to the values found by crystal structure analysis) are the most abundant, accounting for 25.1 % and 26.4% of the surface in **2** and **3**, respectively (Figure 3c,d).

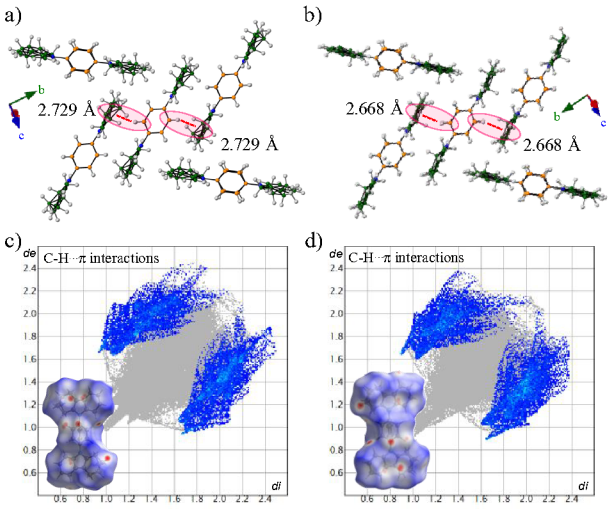

Figure 3. Intermolecular interactions in crystal arrays of **2** and **3** (a and b, respectively). Hirschfeld surface analysis and fingerprints highlighting C-H···π interactions in the crystal packing of **2** and **3** (c and d).

The thermal stability of these compounds was evaluated by TGA-DSC experiments (Figures S5 and S6) and only one endothermic peak associated with the melting point was found in every case (300.8 and 295.4 °C, respectively), confirming similarities in the reticular energy. Even more, purity of the crystalline phases was verified by PXRD for all compounds, and comparisons between experimental and calculated data from LeBail fittings were carried out showing excellent match (Figure S9 and S10). Based on the structural and thermal information, compounds **2** and **3** sustain an isomorphic relationship.[24]

Emissive properties of compounds 1-4

To obtain a wider perspective of the behaviour of the title compounds, UV absorption and fluorescence spectra of the target compounds were recorded first in dilute THF solution (5 x 10^{-6}M), subsequently as aggregates and finally in the solid-state. The absorption bands for compounds **2**, **3**, and **4** with a maximum at 340 nm, indicated that their emission could originate from the same ground state. It is important to note that the maximum absorption in the solid-state was red-shifted compared to that in solution, attributable to molecular aggregation (Table 2).

Photophysical studies as aggregates were also performed to determine whether compounds **2** and **3** show the Aggregation-Induced Emission phenomenon. An increase of the fluorescence by aggregation would indirectly reveal intramolecular motion.[25] To this end, fluorescence experiments for **2** and **3** were carried out in THF solutions using stock solutions (1 mM) and THF-H_2O mixtures (Figure S12 and S13).

The symmetric compound **2** exhibited a strong emissive peak at 365 nm in pure THF, but no AIE was observed. Instead, a steady reduction in the emission intensity was obtained in the f_w range of 0-60%. Subsequently, the fluorescence returned at the initial intensity at f_w = 80 %. Interestingly, the emission of **2** underwent a gradual red shift in the aggregation experiments up to f_w=70% (20 nm), returning to the initial emission with water content above 80%. It seems reasonable to postulate that at the beginning, compound **2** forms some aggregates with only small amount of water, and later when water is the main component, a more emissive aggregate state is produced (*i.e.* nanoparticles). Additional experiments would be needed to prove this statement.

Compound **3** did not show AIE properties under aggregation conditions either. Although a slight increase in the range of f_w=0-20% was observed, a significant quenching occurred afterward. Contrary to compound **2**, the maximum emission of **3** does not change in all the f_w studied. It can be said that quenching of the emission is dominant during these aggregation conditions.[26]

Table 2. Photophysical data for compounds **1-4** in THF solution ([a]naphthalene and [b]phenantrene were used as a standard to determine the quantum yields) and in the solid-state.[c]Taken from ref. 21

Compound	Solution			Solid-state		
	λ Abs (nm)	λ Em (nm)	Φ_F	λ Abs (nm)	λ Em (nm)	Φ_F
1	267	340	0.43[a]	300	371	0.04
2	274	365	0.13[b]	340	369	0.35
3	292	349	0.57[a]	340	372	0.33
4	292	348	0.56[c]	340	404	0.09

After establishing the behavior of **2** and **3** in solution and as aggregates, the fluorescence in the solid-state was determined. It is important to note that the reported fluorophores **1** and **4** have poor solid-state emission, as indicated by their reported quantum yields Φ_F = 0.04 and 0.09, respectively.[21] In the case of **1**, this was ascribed to the restriction of the phenylene rotations, although no evidence of this lack of motion was provided. On the contrary, the dynamic characterization of compound **4** was already reported, but no motion of the phenylene was observed; thus, another nonradiative relaxation channels take place in the latter and quench the emission.

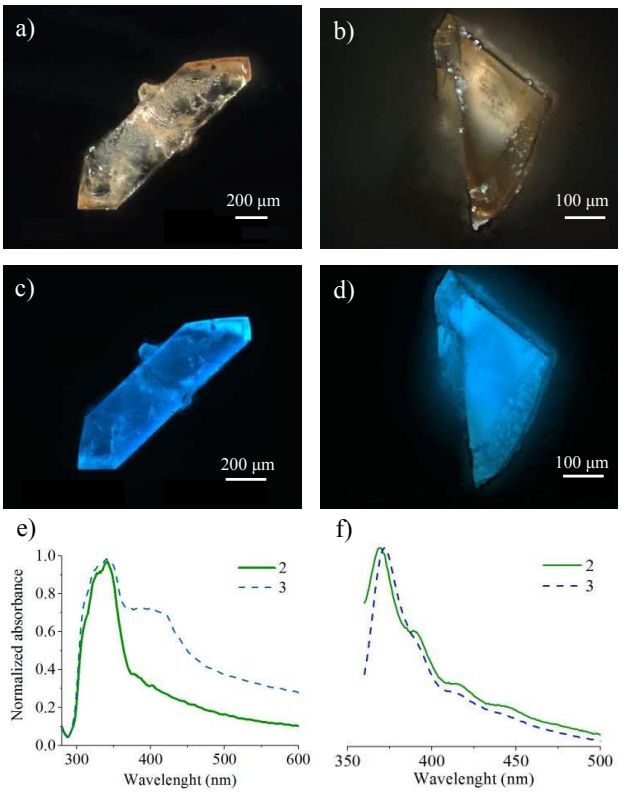

Figure 4. Photographs of single-crystals using confocal microscopy under white light and UV light for compounds **2** (a, c) and **3** (b,d). Comparative normalized absorbance spectra (e) and emission experiments in solid-state (f) for compounds **2** and **3**.

Interestingly, compounds **2** (Φ_F = 0.35) and **3** (Φ_F = 0.33) exhibit higher quantum yields than **1** and **4**. Photographs of single crystals show the blue emission of these compounds (Figures 4a-d). The absorption and emission spectra in the solid-state bear great similarity in the maximum wavelength to solution experiments (Figures 4e-f). Considering only the photophysical data in the solid state, it could be considered that compounds **2** and **3** are more rigid than compounds **1** and **4**, and if so, such rigidification would translate to a better solid-state emission of the title compounds. However, the disordered positions in the X-ray crystallographic data presented above suggested some of intramolecular motion. Therefore, dynamic characterization of the compounds using solid-state NMR was pursued to shed light on the matter.

Characterization of the molecular motion in the solid-state

Solid-state NMR ^{13}C Cross Polarization-Magic Angle Spinning

Considering the disorder in the X-ray crystal structure, we first focused on determining the possible motion of the TCz framework. The most used techniques to explore intramolecular dynamics in the solid-state are: line shape analysis of variable temperature (VT) NMR ^{13}C CPMAS[27] and ^{2}H spin echo[28] spectra. To this end, deuterated analogues were synthesized and crystallized accordingly (Figure S7 and S8).

Variable temperature ^{13}C experiments were carried out first to document the vibrational motion in the aliphatic rings of the tetrahydrocarbazole frameworks (Figure 5a-c). The four carbon atoms from the saturated portion were identified as the overlapped signals in between 23 and 20 ppm at room temperature (Figure 5c). There are two reasons for the signals to overlap, the first and most common is that the magnetic field at 125 MHz is not strong enough for the non-equivalent carbon signals to resolve. The second reason is that this portion could be experiencing rapid conformational rearrangements at 295 K, effectively averaging their crystallographic differences.

The VT ^{13}C CPMAS experiments from 363 to 220 K for compounds **2-*d*$_4$** and **3-*d*$_4$** (Figure S14) show that the intensity and shape of the carbon signals in the aliphatic region are drastically affected as the temperature is reduced. As in any thermally activated process, a lower temperature could 'freeze' the intramolecular motion of the cyclohexene moiety. This indicates that the crystallographic disorder in the TCz is dynamic. Such a conformational process slows down at lower temperatures and in turn, increases the resolution of the spectrum.

From the two title compounds, **2** shows a sharper reduction in signal intensity, as indicated in the I/I_o plot presented in Figure 5b. Unfortunately, a complete splitting of the signals was not achieved even at 220 K, the limit of the spectrometer, although some indications of new signals around 32 and 14 ppm are observed.

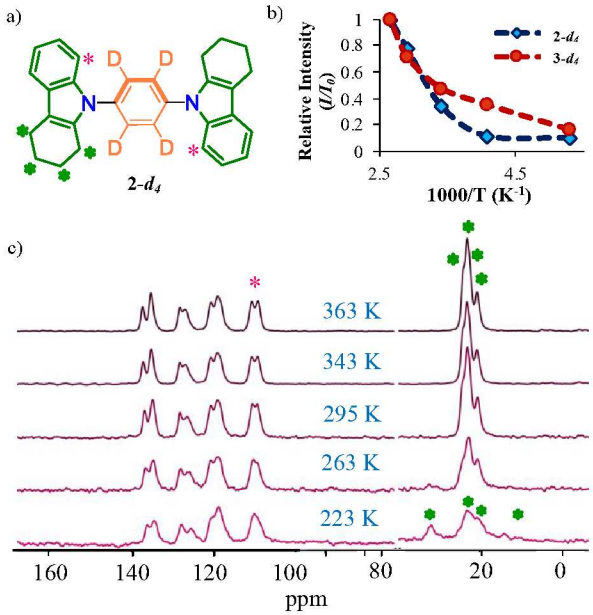

Figure 5. (a) Molecular structure of molecular compound **2-d_4**. (b) A plot of relative intensity (I/I_0) vs 1000/T of compounds **2-d_4** and **3-d_4** considering the peak *ca.* 23 ppm. (c) ^{13}C CPMAS at temperature variable for compound **2-d_4**.

At the same time, most signals in the aromatic region do not suffer significant changes, except the peak at *ca.* 110 ppm assigned to the C8 in the framework (Figure 5a). The asymmetric unit is half of the molecule (Z'=0.5), and only one signal should be observed for this carbon (vide supra). The splitting indicates that the two halves of the structure became crystallographically different above room temperature, suggesting some interaction of this carbon atom with the central phenylene or minute structural changes at high temperature.

Phenylene dynamics by periodic DFT and solid-state ^{2}H NMR experiments

After confirming the motion of cyclohexene in the tetrahydrocarbazole framework, the rotation of the central phenylene was then explored by ^{2}H NMR spin echo.[28] This experiment is governed by the quadrupole moment interaction with the electric field gradient tensor (EFG) over the carbon-deuterium bond. Under the influence of a magnetic field, the nuclear Zeeman interaction gives rise to three energy states for the nuclear spin (I = 1) of deuterium. In crystalline powder, a large number of orientations give rise to a broad line shape known as a Pake pattern. These spectra feature two 'horns' separated by 124-135 kHz for static aromatic deuterons.

Reorientations of the C-^{2}H bond cause a reduction in the separation of the horns and this can be associated to a specific frequency and angular trajectory for the mobile component.[29] The crystalline phase of the deuterated compounds **1-d_4**, **2-d_4**, and **3-d_4** was verified by PXRD (Figure S11). The deuterium experiments of **1-d_4** gave rise to a characteristic line shape known as Pake pattern at all temperatures, from 293 K to 373 K (Figure S15), indicating that the central phenylene in **1** is static.

Although the deuterium NMR spectra of the compounds **2-d_4** and **3-d_4** at 200 K can be considered as static, the line shapes above room temperature were narrower as a result of a complex dynamics.

The combined results obtained from solid-state NMR indicate that the aliphatic portion of the frameworks allowed the motion of the central phenylenes. Periodic DFT computations in the solid-state were carried out to establish the shape of the rotational potential. In both cases, a small energy barrier close to 5 kcal/mol at *ca.* 30° and another barrier of *ca.* 30 kcal closer to 120° were found (Figure 6).

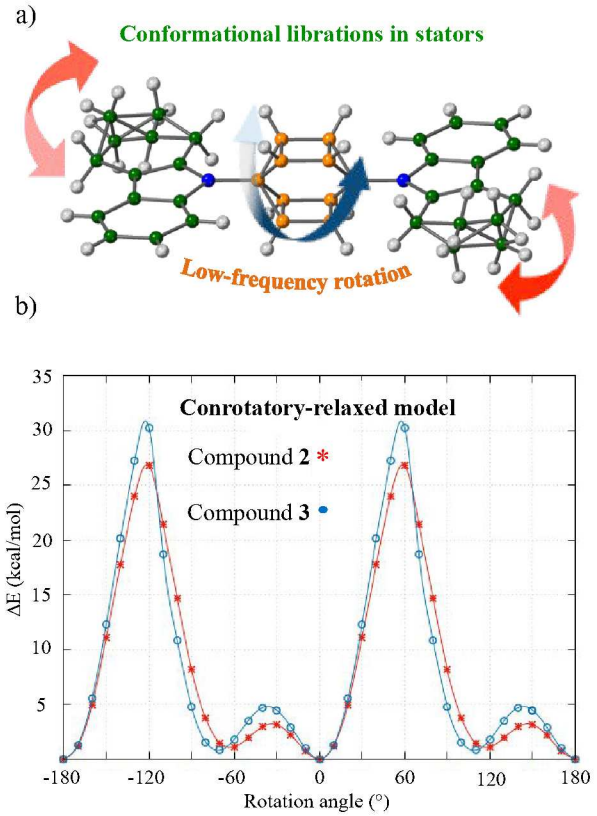

Figure 6. a) Molecular structure of compound **2** illustrating the atomic disorder in its crystal structure b) Computed rotational potential of **2** and **3** using a conrotatory-relaxed model.

A fitting for the ^{2}H line shapes at 200, 300, and 400 K for both compounds was carried out. For this, the asymmetric rotational potential from DFT computations and a previously reported isotropization model were employed.[30] Different rotational frequencies (k_{rot}) were explored until a match with the experimental spectrum was found (Figure 7). The simulated line shapes reflect the frequency of the overall 4-fold process (90° jumps), with low frequency jumps at 300 K and slightly faster jumps at 400 K.

The very high E_a values from DFT computations indicate that the motion at 400 K should be slower, and more importantly, closer to 60 and 100 kHz for **2** and **3**, respectively. Instead, the observed ^{2}H line shape at 400 K was significantly reduced in the case of **2** (fitted K_{rot} = 100 kHz) or showed an isotropic signal in

the case of **3** (fitted K_{rot} = 200 kHz). The NMR data, in combination with the fitting process, indicates that faster motion does occur, and that perhaps the compounds undergo additional structural changes at high temperatures that reduce the activation barriers.

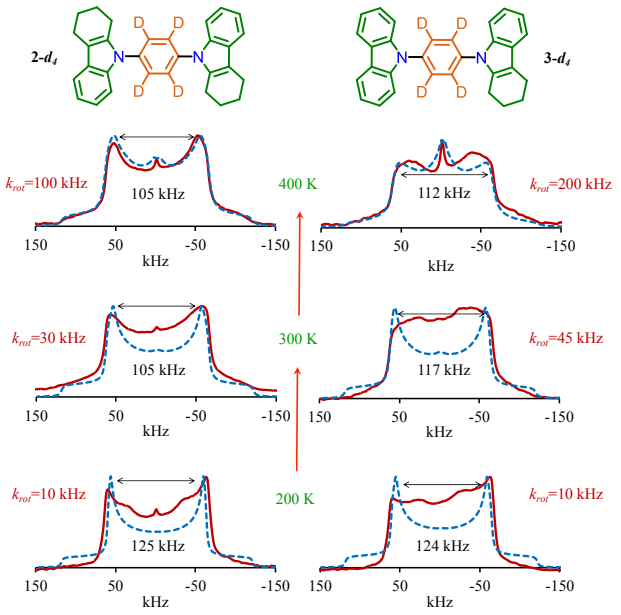

Figure 7. Simulated (dotted line) and experimental (solid red line) ^{2}H NMR line shapes for compounds **2-*d*$_4$** and **3-*d*$_4$**, at 200, 300 and 400 K obtained from a 4-fold asymmetric rotational potential.

Based on the evidence presented here, it can be stated that compounds **1** and **4** do not show neither internal motion nor strong fluorescence in the solid-state. The observed changes in their emission going from solution (0.43 and 0.56, respectively) to the solid-state (0.04 and 0.09, respectively), could come from π-π interactions that quench the emission by the formation of excimers.[31] Alternatively, twisted conformations or extremely fast out-of-plane vibrations may enable other non-radiative pathways. The studies needed to confirm these hypotheses lie beyond the scope of this manuscript.

In contrast, compounds **2** and **3** exhibit good solid-state fluorescence *and* motion in their structures (both in the central phenylene and the tetrahydrocarbazole framework), but the frequency of this motion does not compete with radiative pathways. The restricted access to a conical intersection (RACI) model,[32] may support this statement. This model has been used by Blancafort and coworkers to describe that restricted oscillations (flapping) of phenyl rings in dimethyltetraphenylsilole (DMTPS) cause inaccessible conical intersections, thus enabling the emissive channel.

Conclusions

In summary, we report two new crystalline fluorescent compounds **2** and **3** using 1,2,3,4-tetrahydrocarbazole components as the lattice-forming components. Their photophysical properties were characterized by experiments in solution and in the solid-state. The results were contrasted with previously reported **1** and **4**, revealing strong differences in their properties.

Solid-state NMR ^{13}C CPMAS was used to determine that, opposed to **1** and **4**, the frameworks in **2** and **3** experience rapid conformational rearrangements. Additionally, VT ^{2}H NMR experiments along with DFT computations indicate that the central phenylenes in **2-*d*$_4$** and **3-*d*$_4$** undergo low frequency motions at room temperature with faster dynamics at high temperatures. In both compounds, the slightly different motion is governed by similar intermolecular interactions imposed by the isomorphic crystal array. Compounds **1** and **4** do not feature phenylene motion under similar conditions, although other fast vibrations might still occur. The results here indicate that heterocyclic conjugated compounds could have significant intramolecular motion within their crystals and coexist with good fluorescence in the solid-state.

Conflicts of interest

"There are no conflicts to declare".

Acknowledgements

A.C.-M. thanks Conacyt for the PhD fellowship (576483). This project was supported by PAPIIT (Grant IN209119) and Conacyt (Grant A1-S-32820). We acknowledge the UCLA Department of Chemistry and Biochemistry for solid-state ^{2}H NMR experiments (NSF DMR-1700471 and MRI-1532232). We thank R. A. Toscano, M. C. García González, M. A. Peña, E. Huerta, D. Martínez-Otero and A. Núñez Pineda for technical support. M. Rodriguez-Rivera is acknowledged for solid-state fluorescence measurements. This research was partially supported by Laboratorio Nacional de Ciencias para la Investigación y Conservación del Patrimonio Cultural LANCIC (Instituto de Investigaciones Estéticas). We are also thankful for computer time LANCAD-UNAM-DGTIC-392. The authors thank UNAM for support related to UNAM's BGSI node.

Notes and references

1 S. Erbas-Cakmak, D. A. Leigh, C. T. McTernan, A. L. Nussbaumer, *Chem. Rev*. 2015, **115**, 10081-10206.
2 C. Lemouchi, K. Iliopoulos, L. Zorina, S. Simonov, P. Wzietek, t. Cauchy, A. Rodríguez-Fortea, E. Canadell, J. Kaleta, J. Michl, D. Gindre, M. Chrysos, P. Batail, *J. Am. Chem. Soc.* 2013, **25**, 9366-9376.
3 M. Shi, S.-S. Yu, H. Zhang, S.-X. Liu, H.-B. Duan, *J. Mol. Struct.* 2020, **1206**, 127650.
4 B. R. Arnold, V. Balaji, J. W. Downing, J. G. Radziszewski, J. J. Fisher, J. Michl, *J. Am. Chem. Soc*. 1991, **113**, 2910.
5 N. Tanaka, Y. Inagaki, K. Yamaguchi, W. Setaka, *Cryst. Growth Des.* 2020, **20**, 1097-1102.
6 A. Comotti, S. Bracco, P. Sozzani, *Acc. Chem. Res.* 2016, **49**, 1701−1710.
7 A. Rodríguez-Fortea, E. Canadell, P. Wzietek, C. Lemouchi, M.

Allain, L. Zorina, P. Batail, *Nanoscale*, 2020, DOI: 10.1039/D0NR00858C.
8 M. Jin, S. Yamamoto, T. Seki, H. Ito, M. A. Garcia-Garibay, *Angew. Chem. Int. Ed*. 2019, **58**, 18003-18010.
9 Y. Akune, H. Gontani, R. Hirosawa, A. Koseki, S. Matsumoto, *CrystEngComm,* 2015, **17**, 5789-5800.
10 D. Braga, F. Grepioni, L. Maini, S. d'Agostino, *Eur. J. Inorg. Chem.* 2018, 3597-3605.
11 G. R. Desiraju, *J. Am. Chem. Soc.,* 2013, **135**, 9952–9967.
12 R. C. Ropp, *The chemistry of artificial lighting devices: Lamps, phosphors, and cathode ray tubes*, Elsevier, Amsterdam, 1993.
13 X. Luo, J. Li, C. Li, L. Heng, Y. Q. Dong, Z. Liu, Z. Bo, B. Z. Tang, *Adv. Mater.* 2011, **23**, 3261-3265.
14 N. B. Shustova, T.-C. Ong, A. F. Cozzolino, V. K. Michaelis, R. G. Griffin, M. Dinca, *J. Am. Chem. Soc*. 2012, **134**, 15061−15070.
15 (a) L.-Q. Zheng, S. Yang, J. Lan, L. Gyr, G. Goubert, H. Qian, I. Aprahamian, R. Zenobi, *J. Am. Chem. Soc.* 2019, **141**, 17637-17645. (b) B. Shao, N. Stankewitz, J.-A. Morris, M. D. Liptak, I. Aprahamian, *Chem. Commun.,* 2019, **55**, 9551-9554.
16 Y. Hong, J. W. Y. Lam, B. Z. Tang, *Chem. Soc. Rev.* 2011, **40**, 5361-5388.
17 J. Dong, Y. Pan, H. Wang, K. Yang, L. Liu, Z. Qiao, Y. D. Yuan, S. B. Peh, J. Zhang, L. Shi, H. Liang, Y. Han, X. Li, J. Jiang, B. Liu, D. Zhao, *Angew. Chem. Int. Ed.* 2020, **59**, 2-11.
18 J. Dong, X. Li, K. Zhang, Y. D. Yuan, Y. Wang, L. Zhai, G. Liu, D. Yuan, J. Jiang, D. Zhao, *J. Am. Chem. Soc.* 2018, **140**, 4035-4046.
19 (a) M. E. Howe, M. A. Garcia-Garibay, *J. Org. Chem*. 2019, **84**, 9570-9576. (b) N. L. C. Leung, N. Xie, W. Yuan, Y. Liu, Q. Wu, Q. Peng, Q. Miao, J. W. Y. Lam, B. Z. Tang, *Chem. Eur. J*. 2014, **20**, 15349-15353.
20 Q. Li, S. Yu, Z. Li, J. Qin, *J. Phys. Org. Chem*. 2009, **22**, 241-246.
21 A. Aguilar-Granda, S. Pérez-Estrada, A. E. Roa, J. Rodríguez-Hernández, S. Hernández-Ortega, M. Rodriguez, B. Rodríguez-Molina, *Cryst. Growth Des*. 2016, **16**, 3435-3442.
22 R. Ehama, A. Yokoo, M. Tsushima, T. Yuzuri, H. Suezawa and M. Hirota, *Bull. Chem. Soc. Jpn.,* 1993, **66**, 814–818.
23 C. Janiak, *J. Chem. Soc., Dalton Trans.* 2000, 3885-3896.
24 (a) N. K. Nath, A. Nangia, *Cryst. Growth Des*. 2012, **12**, 5411-5425. (b) A. I. Kitaigorodskii, In Organic Chemical Crystallography; Consultant's Bureau: New York, 1961.
25 S. Liu, Y. Li, H. Zhang, Z. Zhao, X. Lu, J.W.Y. Lam, B. Z. Thang, *ACS Materials Lett.* 2019, **1**, 425-431.
26 L. Zhong, Y. Xie, C. Wang, J.R. Li, Q. Li, Z. Li, *Chem. Commun.*, 2016, **52**, 11496-11499.
27 T. A. V. Khuong, H. Dang, P. D. Jarowski, E. F. Maverick, M. A. Garcia-Garibay*, J. Am. Chem. Soc.* 2007, **129**, 839-845.
28 (a) R. E. Wasylishen, S. E. Ashbrook and S. Wimperis, *NMR of Quadrupolar Nuclei in Solid Materials*, Wiley, Chichester, United Kingdom, 2012. (b) M. J. Duer, *Introduction to Solid-State NMR Spectroscopy*, Blackwell, Oxford, United Kingdom, 2004.
29 L. W. Jelinski, *Ann. Rev. Mater. Sci.* 1985, **15**, 359-377.
30 A. Colin-Molina, M. J. Jellen, E. García-Quezada, M. E. Cifuentes-Quintal, F. Murillo, J. Barroso, S. Pérez-Estrada, R. A. Toscano, G. Merino, B. Rodríguez-Molina, *Chem. Sci.,* 2019, **10**, 4422-4429.
31 Y. Dong, J. W. Y. Lam, A. Qin, Z. Li, J. Sun, H. H. Y. Sung, I. D. Williams and B. Z. Tang, *Chem. Commun*., 2007, 40–42.
32 X.-L. Peng, S. Ruiz-Barragan, Z.-S. Li, Q.-S. Li, L. Blancafort, *J. Mater. Chem. C*, 2016, **4**, 2802.

